On The Lossless Compression of Multidimensional Medical Imagery

Raffaele Pizzolante and Bruno Carpentieri

***Abstract*—** Nowadays, many technologies involved for medical examinations produce multidimensional images. Such data need to be managed in an effective manner in order to be efficiently stored and transmitted. In such scenarios, data compression techniques are essential to improve the efficiency of transmission and storage. Lossless compression techniques are generally preferred, since medical images are often sensitive and important data. Indeed, through lossless compression techniques, the original data can be exactly restored. In this paper, we define a predictive structure well suited for the lossless compression of multidimensional medical images. We experimentally tested our approach on several datasets, including a dataset of 3-D Computed Tomography (CT), 3-D Magnetic Resonance (MR) and 5-D fMRI images. The experimental results we achieved outperform other state-of-the-art approaches for 3-D medical images.

***Keywords*—** Multidimensional medical images compression; Multidimensional medical images coding; Multidimensional data compression.

I. Introduction

NOWADAYS, research activities in medical imaging technologies are continuously evolving on several aspects, especially on the improvement of the acquisition and transmission algorithms.

Internet, Clouds services, Peer-to-Peer networks and all the inter-connection services are widely diffused and provide new services to medical staffs, such as telemedicine, tele-radiology, real-time tele-consultation, PACS (Picture Archiving and Communication Systems), etc.. A significant challenge is related to the efficient management of large amount of storage space, required to store medical data, as well as to the optimization the time required to transmit medical data.

In such scenarios, the implicit costs of required memory space grow proportionally to the size of data. In future medical applications, the new techniques will further increase the requests for memory space and/or transmission time.

Several technologies involved for medical examinations produce multidimensional data. In general, we can informally describe a multidimensional dataset as an N-dimensional collection of highly-related bi-dimensional components (where $N \geq 3$). A component can be an image, a data matrix, etc.. It is important to point out that all of these bi-dimensional components have the same size.

In detail, we can define the *dimensions* of a multidimensional dataset, by using the following notation: $<M_1, M_2, \ldots, M_{N-2}, X, Y>$, where M_f is the size of the f-th dimension ($1 \leq f \leq N-2$), while X and Y are the width and the height of the bi-dimensional components, respectively. A specific bi-dimensional component can be univocally identified through a vector of N–2 elements: $[p_1, p_2, \ldots, p_{N-2}]$, where $p_i \in \{1,2,...,M_i\}$.

The atomic elements of a multidimensional dataset are the *samples*, which are the elements that compose a component. For example, a sample can be a pixel of an image, an element of a matrix, etc.. It should be observed that a sample can be univocally identified, by using the following notation $(d_1, d_2, ..., d_{N-2}, x, y)$, where $1 \leq x \leq X$, $1 \leq y \leq Y$ and $1 \leq d_f \leq D_f$ ($1 \leq f \leq N\text{-}2$).

In medical contexts, *Computed Tomography* (*CT*) and *Magnetic Resonance* (*MR*) imaging technologies produce three-dimensional data ($N = 3$), and *functional Magnetic Resonance* (*fMRI*) imaging technologies produce four-dimensional and five-dimensional data ($N = 4$ and $N = 5$).

In detail, 3-D CT images are acquired through X-rays. In particular, during the acquisition a computer is used, which permits to obtain several cross-sectional views. In addition, for the identification of normal or abnormal structures of the human body, the 3-D CT images are often used. X-rays scanners can generate several images, considering different angles around the body part, which is undergo analysis. The result of the processing, performed by the dedicated computer, is a collection of the cross-sectional images, often referred as slices.

3-D MR images produce relevant information used in medical applications and in medical diagnosis (ranging from neuroimaging to oncology). Generally, MR images are preferred, especially, when both CT and MR images produce the same information. In particular, MR acquisitions do not use any ionizing radiation. On the other hand, MR techniques cannot be used in presence of subjects with cardiac pacemakers and/or metallic foreign bodies, MR techniques

R. Pizzolante is with the Department of Computer Science of University of Salerno, Via Giovanni Paolo II, 132, I-84084 Fisciano (SA), Italy (e-mail: rpizzolante@unisa.it).

B. Carpentieri is with the Department of Computer Science of University of Salerno, Via Giovanni Paolo II, 132, I-84084 Fisciano (SA), Italy (phone: +39 089 969500; fax: +39 089 969600; e-mail: bc@dia.unisa.it).

cannot be applied.

For what concern the *Functional Magnetic Resonance Imaging* (*functional MRI* or *fMRI*), the main aim of such technology is to measure the hemodynamic response (change in blood flow), related to neural activity in the brain [5]. In detail, through fMRI techniques, it is possible to observe the neuronal activities, characterized by neuroactivation task, which need metabolic oxygen support. Substantially, an fMRI scanner is a type of specialized MRI scanner.

It is important to emphasize that each dataset produced by a fMRI scanner produce is composed of a collection of 3-D data volumes (*T* dimension). In particular, a 3-D volume is substantially characterized by a collection (on the *Z* dimension) of bi-dimensional images (*X* and *Y* dimensions). It is important to note that multiple trials of observation are often performed (*R* dimension), in this manner the accuracy of the examination is further improved. Therefore, data can be viewed a multidimensional data, by considering *N* equal to 4 or equal to 5.

It is important to point out that medical data need to be managed in an efficient and effective manner. Starting from such considerations, it is evident that data compression techniques are an essential aid to solve the transmission and storage problems. Lossless compression is often required or indispensable in medical contexts, since such data are precious or often obtained by means of unrepeatable medical exams.

Therefore, this paper focuses on the lossless compression predictive-based techniques [7]. In detail, we have focused on multidimensional medical image sequences (3-D CT and 3-D MR images, and 5-D fMRI images), which need a considerable space memory requirements to be stored or transmitted. We describe a multidimensional and configurable predictive structure, which is well suited for the compression of multidimensional medical images. In addition, our predictor is scalable, adjustable, and adaptive.

The achieved results show experimental evidences of its performance on multidimensional medical images: 3-D Computed Tomography (3-D CT), 3-D Magnetic Resonance (3-D MR) and 5-D functional Magnetic Resonance Images (5-D fMRI).

The rest of this paper is organized as follows: Section 2 describes the predictive structure, Section 3 reports our experimental results and Section 4 highlights our conclusions and outlines future research directions.

II. Predictive Coding of Multidimensional Images

The proposed predictive model is based on the least squares optimization techniques. The prediction is performed by considering a multidimensional prediction context, which is composed by the neighboring samples of the current component and one (or more) reference component(s). It is important to note that the reference component(s) can be of different dimension(s), with respect to the current component. Thus, the prediction of the current sample is obtained by using a multidimensional prediction context.

From now on, without loss of generality, we assume that the current sample has coordinates (m_1, m_2, …, m_{N-2}, x, y) (where $1 \le m_1 \le M_i$, $1 \le x \le X$ and $1 \le y \le Y$).

We denote as *Sets of References*, the reference components used by our predictor. The Sets of References should be set at the beginning of the algorithm.

In particular, each Set of References is defined as in the equation (1).

$$R_i = \{r_1^i, r_2^i, ..., r_{t_i}^i\} \ (i \in \{1,2,...,N-2\}) \quad (1)$$

In the equation (1), each element is defined as $r_j^i \in \{1,2,...,M_i\} \cup \{-1,-2,...,-M_i\}$, $t_i = |R_i|$, $1 \le j \le t_i$, and $\left|\bigcup_{i=1}^{N-2} R_i\right| > 0$.

A generic element of a Set of References, $r_j^i \in R_i$ ($1 \le i \le N-2$), denotes a specific bi-dimensional component. In particular, we will use the following notation: if $r_j^i > 0$, then the denoted component is the one identified through the vector $[m_1, m_2, ..., m_{i-1}, r_j^i, m_{i+1}, ..., m_{N-2}]$, or, if $r_j^i < 0$, then the denoted component is the one identified through the vector $[m_1, m_2, ..., m_{i-1}, m_i - |r_j^i|, m_{i+1}, ..., m_{N-2}]$.

We define an *enumeration*, in order to refer to a sample, without the use of its absolute coordinates. In detail, through an enumeration the relative indexing among all the samples (or a subset of them) of the same component is allowed. In particular, by fixing a sample, namely the *reference sample*, all the other samples of the component will be indexed with respect to it. The relative indexing of the samples is used for the definition of the multidimensional prediction context involved by our predictive model.

Let *E* denotes a 2-D enumeration, which has as objective the relative indexing of the samples in a bi-dimensional context, with respect to a specific reference sample. The fundamental requisites that the enumeration *E* needs to satisfy are that the specified reference sample has 0 as index and that any two samples (with different coordinates) do not have the same index.

Let $x_j^{(e)}(r_s^j)$ (where $r_s^j \in R_j$) denotes the *e*-th sample in the bi-dimensional context according to the enumeration *E* with respect to the sample with coordinate (m_1, m_2, …, m_{j-1}, r_s^j, m_{j+1}, …, m_{N-2}, x, y) when $r_s^j > 0$, or (m_1, m_2, …, m_{j-1}, $m_j - |r_s^j|$, m_{j+1}, …, m_{N-2}, x, y) when $r_s^j < 0$.

Furthermore, let $x^{(e)}$ denotes the *e*-th sample, according to the enumeration *E*, with respect to the current sample. Notice that $x^{(0)}$ denotes precisely the current sample.

In particular, the *T*-order prediction (where $T = \sum_{i=1}^{N-2} t_i = \sum_{i=1}^{N-2} |R_i|$) of the current sample $x^{(0)}$ is obtained by means of the equation (2).

$$\hat{x}^{(0)} = \sum_{i=1}^{N-2} \sum_{j=1}^{t_i} \alpha_i^j \cdot x_i^{(0)}(r_j^i) \quad (2)$$

The $\alpha_0 = [\alpha_1^1,...,\alpha_1^{t_1},...,\alpha_i^1,...,\alpha_i^{t_i},...,\alpha_{N-2}^1,...,\alpha_{N-2}^{t_{N-2}}]^t$ coefficients are chosen to minimize the energy of the prediction error (equation (3)).

$$P = \sum_{i=1}^{H} \left(x^{(i)} - \hat{x}^{(i)}\right)^2 \quad (3)$$

It should be noted that the *H* parameter is used to indicate the number of samples used, for the current and for each of the components specified in the references sets. Therefore, it is observable that $H \cdot (T + 1) + T$ samples are used for each prediction.

The coefficients α_0 are obtained by using the optimal linear prediction method, as in [10]. We can rewrite the equation (3), by using the matrix form as outlined in the equation (4).

$$P = (\boldsymbol{C}\alpha - \boldsymbol{X})^t \cdot (\boldsymbol{C}\alpha - \boldsymbol{X}) \quad (4)$$

As in [10], the linear system, reported in the equation (5), is obtained by taking the derivate of the equation (4), with respect to α, and by setting it to zero.

$$(\boldsymbol{C}^t\boldsymbol{C})\ \alpha_0 = (\boldsymbol{C}^t\boldsymbol{X}) \quad (5)$$

Once the coefficients α_0, which solve the linear system (5), are obtained, it is possible to determinate the prediction of the current sample, $\hat{x}^{(0)}$, by using the equation (2).

The prediction error, obtained by means of the equation (6) and eventually mapped through an invertible mapping function [7] is sent to an entropy encoder.

$$e = \left\lfloor x^{(0)} - \hat{x}^{(0)} \right\rfloor \quad (6)$$

If our predictive structure uses only past information, there is no need to send any side information to the decompression algorithm.

It is important to emphasize that the computational complexity of the prediction is related to the two configurable parameters: *H* and the Sets of References. It is possible to model the multidimensional prediction context by specifying its wideness and the number of the reference components. By doing this it is possible either to define a prediction context which can minimize the use of the computational resources or to refine the accurateness of the prediction by using more computational resources.

In some situations, our predictive structure can be ineffective. In particular, when the linear system of equations (3) cannot be solved because it has no solutions or infinitely many solutions. In such scenarios, which we referred as *exceptions*, the predictive structure is not able to perform the prediction.

In presence of a sample that cannot be predicted through the proposed predictive structure (because an exception is verified), an alternative predictive structure (as for instance Median Predictor, etc.) shall be used.

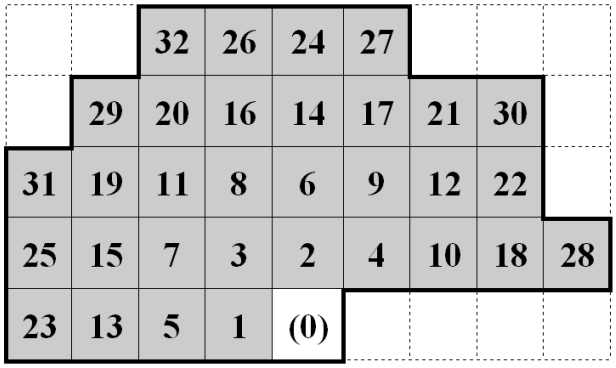

Fig. 1. Graphical representation of the used enumeration.

III. Experimental Results

In this section, we describe the experimental results achieved during our testing phase. In particular, we experimentally performed our testing on several datasets related to different typologies of multidimensional medical images: 3-D medical images (Section 3.A), namely, 3-D Computed Tomography images and 3-D Magnetic Resonance images, and 5-D fMRI images (Section 3.B).

It is important to note that the predictive-based compression scheme, we implemented, predicts each sample by including only the previously coded samples, in the prediction context. In this manner, both the compression and the decompression algorithms are able to have a consistent prediction for each sample. Each prediction is followed by the coding of the prediction error, which is obtained as the difference between the current sample and its prediction. It is important to point out that the prediction errors can be encoded by using an entropy or a statistical coder.

In our experiments, the following encoders, for the prediction of errors, are used: *PAQ8* [6] and/or Prediction by *Partial Matching with Information Inheritance* (*PPMd* or *PPMII*) [11]. In addition, different values for the *H* parameter and several values for the Sets of References are considered.

It is important to point out that all the samples that belong to a component, with no reference component(s), are predicted by using the *2-D Linearized Median Predictor* (*2D-LMP*) (described in [9]). On the other hand, for all the other samples that belong to the components with reference component(s), our multidimensional predictive structure is used.

The enumeration we used is graphically represented in Figure 1, in which the current sample has zero as index (highlighted in parenthesis), while the grey samples are already processed.

In the following, when we mention a Set of Reference, the mnemonic name of a dimension is used, instead of its index, in order to improve the readability. For instance, we use the notation of R_Z to indicate the Set of Reference related to the *Z* dimension.

All the results are reported in terms of *bits-per-sample* (*BPS*).

Tab. 1. Description of the 3-D CT images.

Image Name	Number of Slices
CT_skull	192
CT_wrist	176
CT_carotid	64
T_Aperts	96

Tab. 2. Description of the 3-D MR images.

Image Name	Number of Slices
MR_liver_t1	48
MR_liver_t2e1	48
MR_sag_head	48
MR_ped_chest	64

Tab. 3. Experimental results achieved on the 3-D CT images. PPMd is used for the coding of prediction errors.

H	$R_Z = \{-1\}$	$R_Z = \{-1,-2\}$	$R_Z = \{-1,-2,-3\}$
CT_Aperts			
H=8	0.8507	0.7870	0.8140
H=16	0.8646	0.7768	0.7850
H=32	0.8751	0.7778	0.7786
CT_carotid			
H=8	1.4535	1.4208	1.4130
H=16	1.4770	1.4128	1.3650
H=32	1.4850	1.4052	1.3455
CT_skull			
H=8	2.1417	1.7159	1.7260
H=16	2.1552	1.6604	1.6237
H=32	2.1603	1.6287	1.5735
CT_wrist			
H=8	1.0958	1.0562	1.0521
H=16	1.1109	1.0129	0.9674
H=32	1.1129	0.9895	0.9344

A. 3-D Medical Images

We performed our experiments on a dataset composed by four 3-D CT (briefly described in Tables 1) and four 3-D MR images (briefly described in Tables 2). In particular, each slice have 256 columns and 256 rows. In addition, each sample is stored by using 8 bits.

Regarding the coding of prediction errors, we have used either the PAQ8 algorithm as well as the PPMd algorithm. It is important to note that the error is first mapped, similarly to [7], before the sending to the encoder. In addition, the *3-D Differences-based Linearized Median Predictor* (3D-DLMP) [9] is used for the exceptions. In relation to the *H* parameter, the following parameters are used: 8, 16 and 32. Furthermore, several configurations for the Set of References are used.

Tables 3 and 4 report the experimental results achieved on the 3-D CT images and 3-D MR images, respectively. In particular, two configurations of the Set of References are used and the prediction of errors are coded through the PPMd scheme.

Analogously to Tables 3 and 4, Tables 5 and 6 respectively summarize the results achieved on the 3-D CT images and on the 3-D MR images, in which the PAQ8 scheme is used for the coding of prediction errors,

Tab. 4. Experimental results achieved on the 3-D MR images. PPMd is used for the coding of prediction errors.

H	$R_Z = \{-1\}$	$R_Z = \{-1,-2\}$	$R_Z = \{-1,-2,-3\}$
MR_liver_t1			
H=8	2.2970	2.0224	2.0722
H=16	2.3295	1.9804	1.9563
H=32	2.3618	1.9731	1.9231
MR_liver_t2e1			
H=8	1.9721	1.4332	1.4240
H=16	2.0014	1.4073	1.3619
H=32	2.0186	1.3930	1.3366
MR_ped_chest			
H=8	1.6736	1.5245	1.5197
H=16	1.6856	1.4587	1.3956
H=32	1.6952	1.4282	1.3391
MR_sag_head			
H=8	2.0916	1.7127	1.7061
H=16	2.0992	1.6750	1.6308
H=32	2.1049	1.6477	1.5892

Tab. 5. Experimental results achieved on the 3-D CT images. PAQ8 is used for the coding of prediction errors.

H	$R_Z = \{-1\}$	$R_Z = \{-1,-2\}$	$R_Z = \{-1,-2,-3\}$
	CT_Aperts		
H=8	0.7829	0.7268	0.7501
H=16	0.7968	0.7198	0.7261
H=32	0.8063	0.7205	0.7198
	CT_carotid		
H=8	1.3838	1.3456	1.3376
H=16	1.4060	1.3417	1.2930
H=32	1.4116	1.3343	1.2739
	CT_skull		
H=8	2.0291	1.6139	1.6191
H=16	2.0365	1.5645	1.5247
H=32	2.0372	1.5366	1.4786
	CT_wrist		
H=8	1.0496	1.0066	0.9998
H=16	1.0645	0.9691	0.9244
H=32	1.0646	0.9486	0.8935

Tab. 6. Experimental results achieved on the 3-D MR images. PAQ8 is used for the coding of prediction errors.

H	$R_Z = \{-1\}$	$R_Z = \{-1,-2\}$	$R_Z = \{-1,-2,-3\}$
	MR_liver_t1		
H=8	2.2013	1.9443	1.9870
H=16	2.2304	1.9062	1.8823
H=32	2.2568	1.8973	1.8485
	MR_liver_t2e1		
H=8	1.8760	1.3437	1.3311
H=16	1.9051	1.3196	1.2739
H=32	1.9201	1.3079	1.2504
	MR_ped_chest		
H=8	1.5801	1.4576	1.4577
H=16	1.5869	1.3917	1.3406
H=32	1.5932	1.3591	1.2822
	MR_sag_head		
H=8	1.9606	1.5960	1.5888
H=16	1.9676	1.5609	1.5179
H=32	1.9720	1.5360	1.4768

In Tables 7 and 8, the average results related to 3-D CT images and 3-D MR images are respectively reported. It should be noted that the best results are achieved when the PAQ8 algorithm is used. However, the PAQ8 scheme needs more computational resources with respect to the PPMd scheme.

From Figures 2 and 3, which show the histograms respectively related to Tables 7 and 8, the best trend of the average results is obtained when the *H* parameter is equal to 32, except for the configuration in which R_Z={-1} (i.e., one previous slice is used). In detail, the best results are obtained when the configuration R_Z={-1,-2,-3} is used (i.e., three previous slices are used).

Tab. 7. Average experimental results on the 3-D CT images.

H	$R_Z = \{-1\}$	$R_Z = \{-1,-2\}$	$R_Z = \{-1,-2,-3\}$
	PPMd		
H=8	1.3854	1.2450	1.2513
H=16	1.4019	1.2157	1.1853
H=32	1.4083	1.2003	1.1580
	PAQ8		
H=8	1.3114	1.1732	1.1767
H=16	1.3260	1.1488	1.1171
H=32	1.3299	1.1350	1.0915

Tab. 8. Average experimental results on the 3-D MR images.

H	$R_Z = \{-1\}$	$R_Z = \{-1,-2\}$	$R_Z = \{-1,-2,-3\}$
	PPMd		
H=8	2.0086	1.6732	1.6805
H=16	2.0289	1.6304	1.5862
H=32	2.0451	1.6105	1.5470
	PAQ8		
H=8	1.9045	1.5854	1.5912
H=16	1.9225	1.5446	1.5037
H=32	1.9355	1.5251	1.4645

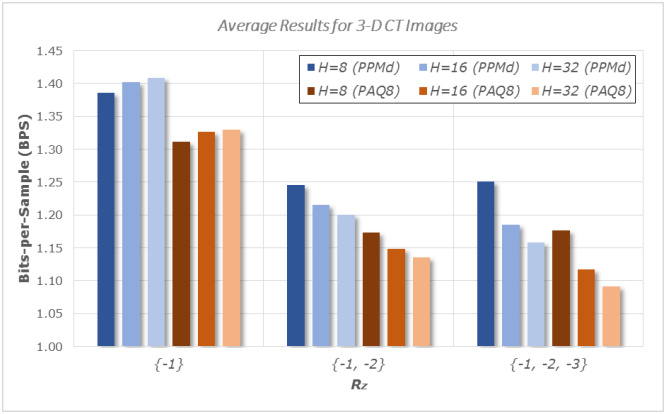

Fig. 2. Histogram of Table 7.

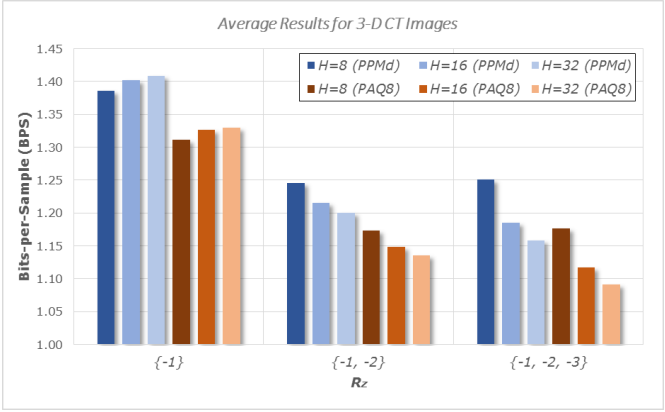

Fig. 3. Histogram of Table 8.

Tab. 9. Comparison of different compression techniques on the 3-D CT images.

Methods / Images	CT_skull	CT_wrist	CT_carotid	CT_Aperts
Proposed (H=32)	1.5393	0.9527	1.3363	0.7265
Proposed (H=16)	1.5688	0.9737	1.3448	0.7271
3D-ESCOT [12]	1.8350	1.0570	1.3470	0.8580
MILC [9]	2.0306	1.0666	1.3584	0.8190
AT-SPIHT [4]	1.9180	1.1150	1.4790	0.9090
3D-CB-EZW [2]	2.0095	1.1393	1.3930	0.8923
DPCM+PPMd [1]	2.1190	1.0290	1.4710	0.8670
3D-SPIHT [12]	1.9750	1.1720	1.4340	0.9980
3D-EZW [2]	2.2251	1.2828	1.5069	1.0024
JPEG-LS [3]	2.8460	1.6531	1.7388	1.0637

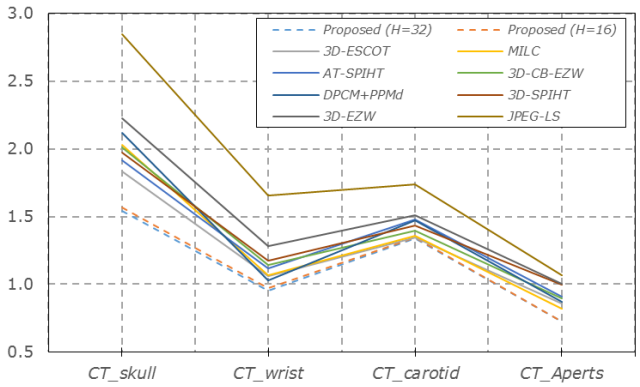

Fig. 4. Graphical comparison of different compression techniques on the 3-D CT images.

Tab. 10. Comparison of different compression techniques on the 3-D MR images.

Methods / Images	MR_liver_t1	MR_liver_t2e1	MR_sag_head	MR_ped_chest
Proposed (H=32)	1.8996	1.3101	1.5477	1.3740
Proposed (H=16)	1.9089	1.3232	1.5737	1.4053
3D-ESCOT	2.0760	1.5100	1.9370	1.6180
MILC	2.1968	1.7590	2.0975	1.6556
3D-SPIHT	2.2480	1.6700	2.0710	1.7420
3D-CB-EZW	2.2076	1.6591	2.2846	1.8705
DPCM+PPMd	2.3900	2.0250	2.1270	1.6890
3D-EZW	2.3743	1.8085	2.3883	2.0499
JPEG-LS	3.1582	2.3692	2.5567	2.9282

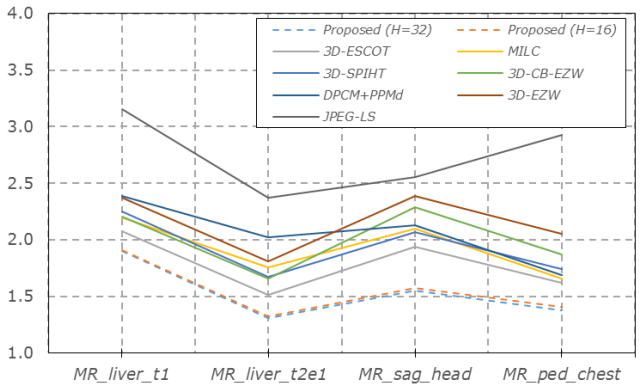

Fig. 5. Graphical comparison of different compression techniques on the 3-D MR images.

In Table 9, we compare the achieved experimental results with respect to the state of the art techniques (first column), for each one of the tested 3-D CT images (from the second to the fifth columns). It is important to note that we report the results obtained by our approach, by using H = 32 (first row) and H = 16 (second row). In detail, the configuration R_Z = {-1, -2} is used, whereas the PAQ8 scheme is used for the coding of prediction errors. Figure 4 graphically shows the results reported in Table 9, by emphasizing our approach with dotted lines (cyan dotted line when H = 16 and orange dotted line for H = 32, respectively). In particular, on the X-axis are reported the 3-D CT images, while on the Y-axis the obtained results value, in terms of BPS. From Figure 5, it should be noted that our approach outperforms all the compared state-of-the-art methods.

Table 10, similarly to Table 9, summarizes the comparison of the achieved experimental results with respect to the state of the art techniques, for what concern the 3-D MR images. Also for the 3-D MR images, we compare the results obtained by our approach, in which H = 32 (first row) and H = 16 (second row) are used. In particular, the configuration R_Z = {-1, -2} is used and the PAQ8 scheme is used for the coding of prediction errors. From Figure 5, which graphically shows the results reported in Table 10, it is possible to observe that our approach outperforms all the compared methods.

B. 5-D fMRI Images

Now, we focus on the experiments we performed on the data produced through the functional Magnetic Resonance Imaging (fMRI) technology. In particular, we perform our experiments on a dataset, denoted as *"Living-nonliving decision with plain or mirror-reversed text"* (briefly outlined in Table 11), provided by the *OpenfMRI project* [8].

For brevity, we used a more compact notation that permits to indicate which dimensions will be used by the predictive structure for each prediction. For example, the following notation *4-D (T, Z)* is related to a specific configuration of the Sets of References (i.e., R_T = {-1} and R_Z = {-1}). In particular, such an example indicates that the previous slice of each one of four dimensions of a fMRI image, namely, the dimensions highlighted in parenthesis (i.e., T and Z dimensions) and the X and the Y dimensions. Only for the configuration denoted as *5-D*, it is no necessary to report the used dimensions in the parenthesis, because of all of the dimensions of a fMRI image are exploited (i.e., R_R = {-1}, R_T = {-1} and R_Z = {-1}).

In detail, for our experiments we used the 2D-LMP predictor for the prediction of all samples that belong to the components, with no reference component(s), as well as for the management of the exceptions. In addition, all the prediction errors are coded by using the PPMd scheme.

Tables 12 and 13 report the experimental results related to the *H* parameter equal to 16 and 32, respectively.

Tab. 11. Description of the dataset of 5-D fMRI Images.

Subjects	Dimension
sub001	<6, 205, 25, 64, 64>
sub002	<6, 205, 25, 64, 64>
sub003	<5, 205, 25, 64, 64>
sub004	<6, 205, 25, 64, 64>
sub005	<5, 205, 25, 64, 64>
sub006	<5, 205, 25, 64, 64>
sub007	<5, 205, 25, 64, 64>
sub008	<6, 205, 25, 64, 64>
sub009	<6, 205, 25, 64, 64>
sub010	<6, 205, 25, 64, 64>
sub011	<6, 205, 25, 64, 64>
sub012	<6, 205, 25, 64, 64>
sub013	<6, 205, 25, 64, 64>
sub014	<6, 205, 25, 64, 64>

Tab. 12. Experimental results achieved on the dataset of fMRI Images (*H* = 16).

Subjects	**3-D (*Z*)**	**3-D (*T*)**	**4-D (*Z*, *T*)**	**4-D (*T*, *R*)**	**5-D**
sub001	7.0516	5.7572	5.7733	5.7470	5.7947
sub002	7.0821	5.6136	5.6337	5.5941	5.6437
sub003	7.4694	5.7476	5.7815	5.7176	5.7750
sub004	7.4131	5.7105	5.7421	5.6716	5.7301
sub005	7.2722	5.6545	5.6868	5.6376	5.6952
sub006	6.7544	5.3380	5.3642	5.3047	5.3567
sub007	7.0456	5.5538	5.5845	5.5156	5.5710
sub008	7.1395	5.6751	5.7029	5.6330	5.6871
sub009	6.9110	5.5133	5.5368	5.4786	5.5300
sub010	7.3647	5.6765	5.7113	5.6262	5.6854
sub011	7.2444	5.6330	5.6649	5.6201	5.6769
sub012	7.0564	5.6360	5.6597	5.5670	5.6160
sub013	7.5621	5.9086	5.9427	5.8603	5.9201
sub014	7.0872	5.6808	5.7040	5.6362	5.6871

Tab. 13. Experimental results achieved on the dataset of fMRI Images (H = 32).

Subjects	**3-D (*Z*)**	**3-D (*T*)**	**4-D (*Z*, *T*)**	**4-D (*T*, *R*)**	**5-D**
sub001	7.0477	5.7362	5.7233	5.7010	5.7094
sub002	7.0824	5.5935	5.5861	5.5494	5.5615
sub003	7.4737	5.7266	5.7299	5.6721	5.6896
sub004	7.4146	5.6894	5.6913	5.6254	5.6443
sub005	7.2689	5.6322	5.6352	5.5919	5.6105
sub006	6.7531	5.3145	5.3119	5.2573	5.2712
sub007	7.0429	5.5313	5.5321	5.4700	5.4858
sub008	7.1366	5.6520	5.6505	5.5857	5.6009
sub009	6.9099	5.4903	5.4845	5.4311	5.4431
sub010	7.3692	5.6549	5.6593	5.5796	5.5987
sub011	7.2383	5.6100	5.6122	5.5723	5.5895
sub012	7.0516	5.6128	5.6061	5.5186	5.5282
sub013	7.5576	5.8844	5.8862	5.8113	5.8283
sub014	7.0776	5.6562	5.6497	5.5862	5.5976

Tab. 14. Average experimental results on the fMRI images.

H	**3-D (*Z*)**	**3-D (*T*)**	**4-D (*Z*, *T*)**	**4-D (*T*, *R*)**	**5-D**
8	7.1809	5.6872	5.7795	5.7053	5.8118
16	7.1753	5.6499	5.6777	5.6150	5.6692
32	7.1732	5.6275	5.6256	5.5680	5.5828

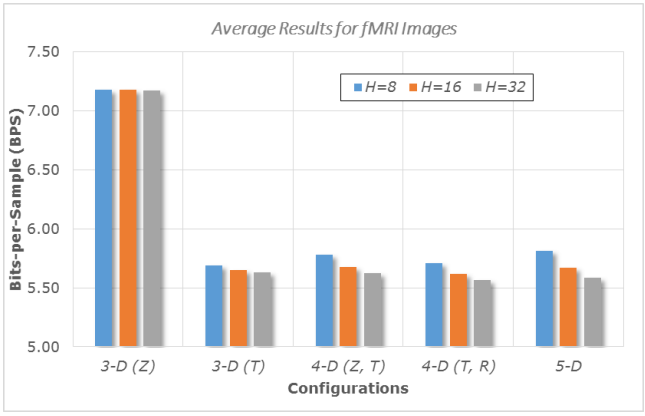

Fig. 6. Histogram of Table 12.

In Table 14, the average experimental results related to the dataset of fMRI images are reported.

From Figure 6 (which graphically represents the results in Table 14), it is possible to note that the worst results are obtained in the case of the *3-D (Z)* configuration. On the other hand, the best results are achieved when the *4-D (T, R)* configuration is used.

In the case of the *4-D (T, Z)* configuration, the achieved average results are slightly better with respect to the ones obtained when the *3-D (T)* configuration is used, but only in the case in which the *H* parameter is equal to 32. Indeed, the results of the *4-D (T, Z)* configuration are worse than the ones of the *3-D (T)* configuration, when the *H* parameter is equal to 16.

IV. Conclusions and Future Work

Various medical instruments produce multidimensional medical images (i.e., magnetic resonance, computed tomography, etc.). Such data are often transmitted among different entities and should be manage in an efficient manner.

Data compression techniques are an essential aid to solve the transmission and storage problems. By considering the importance of such typology of data, lossless techniques are often preferred, since the lost information, due to lossy techniques, might lead to incorrect analysis.

In this paper, we have described a Multidimensional Predictive Model that can be used for efficient and lossless compression of multidimensional medical images. Our predictive model is configurable and it is also possible to configure it, according to the hardware in which the compression algorithm is implemented.

We have experimentally tested our approach by considering several datasets composed by 3-D magnetic resonance (MR), 3-D computed tomography (CT) and 5-D fMRI images. The

achieved results related to the 3-D medical images outperform the compared state of the art techniques.

Future works will include a deeper experimentation on lossless compression by using other *N*-D data (eg. 4-D ultrasound images, etc.).

REFERENCES

[1] S. Ait-Aoudia, F. Benhamida, M. Yousfi, "Lossless Compression of Volumetric Medical Data", in *Lecture Notes in Computer Science*, 4263/2006, 2006, pp. 563–571.

[2] A. Bilgin, G. Zweig, and M.W. Marcellin, "Three-Dimensional Image Compression with Integer Wavelet", in *Applied Optics*, 39(11), pp. 1799–1814, 2000.

[3] B. Carpentieri, M. Weinberger, G. Seroussi, "Lossless Compression of Continuous Tone Images", in *Proceeding of IEEE*, 88, 11, pp. 1797–1809, 2000.

[4] S. Cho, D. Kim, W.A. Pearlman, "Lossless Compression of Volumetric Medical Images with Improved Three-Dimensional SPIHT Algorithm", in *Journal of Digital Imaging*, 17(1), 57–63, 2004.

[5] A. Castiglione, A. De Santis, R. Pizzolante, A. Castiglione, V. Loia, F. Palmieri, "On the Protection of fMRI Images in Multi-domain Environments", in *Proceedings of Advanced Information Networking and Applications (AINA)*, pp. 476–481, 2015.

[6] B. Knoll, N. de Freitas, "A Machine Learning Perspective on Predictive Coding with PAQ8" in *Proceedings of Data Compression Conference (DCC)*, Snowbird, UT, USA, pp. 377–386, 2012.

[7] G. Motta, J.A. Storer, B. Carpentieri, "Lossless Image Coding via Adaptive Linear Prediction and Classification", in *Proceedings of the IEEE*, 88 (11), pp. 1790–1796, 2000.

[8] OpenfMRI Site, Available on: https://openfmri.org (Accessed on Sep. 2015).

[9] R. Pizzolante, B. Carpentieri, "Lossless, low-complexity, compression of three-dimensional volumetric medical images via linear prediction", in *Proceedings of Digital Signal Processing (DSP)*, pp. 1–6, 2013.

[10] F. Rizzo, B. Carpentieri, G. Motta, J.A. Storer, "Low-complexity lossless compression of hyperspectral imagery via linear prediction", in *Signal Processing Letters, IEEE*, 12 (2), pp. 138–141, 2005.

[11] D. Shkarin, "PPM: one step to practicality", in *Proceedings of Data Compression Conference (DCC)*, Snowbird, USA, pp. 202–211, 2002.

[12] Z. Xiong, X. Wu, S. Cheng, H. Jianping, "Lossy-to-lossless compression of medical volumetric data using three-dimensional integer wavelet transforms", in *IEEE Trans. on Medical Imaging*, 22(3), pp. 459-470 2003.

Bruno Carpentieri received the "Laurea" degree in Computer Science from the University of Salerno, Salerno, Italy, and the M.A. and Ph.D. degrees in Computer Science from the Brandeis University, Waltham, MA, U.S.A. Since 1991, he has been first Assistant Professor and then Associate Professor of Computer Science at the University of Salerno (Italy). His research interests include lossless and lossy image compression, video compression and motion estimation, information hiding.

He has been, from 2002 to 2008, Associate Editor of the journal IEEE Trans. on Image Processing. He was recently chair and organizer of the International Conference on Data Compression, Communication and Processing 2011, co-chair of the International Conference on Compression and Complexity of Sequences, and, for many years, program committee member of the IEEE Data Compression Conference and of other international Conferences in the field. He has been responsible for various European Commission contracts regarding image and video compression.

Raffaele Pizzolante received his Master degree (cum laude) in Computer Science from University of Salerno (Italy) in 2011. Currently, he continues his studies as a Ph.D. student at the same university. His research interests include Data Compression, Image Processing, Digital Watermarking and Information Hiding.